

**A SENSITIVE VLA SEARCH FOR SMALL-SCALE GLYCINE EMISSION  
TOWARD OMC-1**

J. M. Hollis<sup>1</sup>, J. A. Pedelty <sup>2</sup>, L. E. Snyder<sup>3</sup>, P. R. Jewell<sup>4</sup>, F. J. Lovas<sup>3,5</sup>, Patrick Palmer<sup>6</sup>,  
and S.-Y. Liu<sup>7,8</sup>

<sup>1</sup>Earth and Space Data Computing Division, Code 930, NASA Goddard Space Flight  
Center, Greenbelt, MD 20771

<sup>2</sup>Biospheric Sciences Branch, Code 923, NASA Goddard Space Flight  
Center, Greenbelt, MD 20771

<sup>3</sup>Department of Astronomy, University of Illinois, 1002 W. Green Street,  
Urbana, IL 61801

<sup>4</sup>National Radio Astronomy Observatory, P. O. Box 2, Green Bank, WV 24944-0002

<sup>5</sup>Current address: National Institute of Standards & Technology, 100 Bureau Drive,  
Stop 8441, Gaithersburg, MD 20899-8441

<sup>6</sup>Department of Astronomy and Astrophysics, University of Chicago, 5640 South Ellis  
Avenue, Chicago, IL 60637

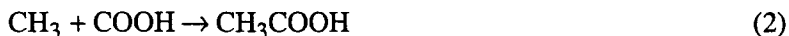
<sup>7</sup>Department of Astronomy, California Institute of Technology, Pasadena, CA 91125

<sup>8</sup>Current address: Institute of Astronomy and Astrophysics, Academia Sinica,  
P.O. Box 23-141, Taipei 106, Taiwan, R.O.C.

**Subject headings:** ISM: abundances --- ISM: clouds ---  
ISM: individual (Orion Molecular Cloud) ---  
ISM: molecules --- radio lines: ISM

## 1. INTRODUCTION

Recent laboratory experiments demonstrate the synthesis of amino acids, a basic constituent of life, when ice mixtures representative of interstellar grain mantles were subjected to UV radiation at temperatures below 15 K. Bernstein et al. (2002) produced amino acids in a water-rich ice environment, while similar results were achieved by Muñizo Caro et al. (2002) in a water-poor ice environment. Sorrell (2001) suggests glycine could be produced from simple interstellar species that undergo radical-molecule interactions when excess reaction heat is available to overcome the activation barrier. Sorrell (2001) proposes the following reaction sequence may occur in grain mantle sites:



Such interactions would require high concentrations of requisite radicals and molecules that may be present in such sites. Moreover, acetic acid ( $\text{CH}_3\text{COOH}$ ) has now been detected in two interstellar clouds: SgrB2(N-LMH) and W51 (Mehringer et al. 1997; Remijan et al. 2002). Another possible route for producing glycine is a combination of gas-grain chemistry involving formic acid ( $\text{HCOOH}$ ), a known interstellar molecule, and the amino-alcohol ( $\text{NH}_2\text{CH}_2\text{OH}$ ) which has been identified as a component of Comet Halley dust (Kissel & Krueger 1987). Protonated glycine is produced in an endothermic reaction (Charnley, Ehrenfreund, & Kuan 2001) which would find favorable conditions in hot molecular cores:



Additional support for the probable existence of interstellar glycine is provided by the recent detections of interstellar glycolaldehyde ( $\text{CH}_2\text{OHCHO}$ ) and ethylene glycol ( $\text{HOCH}_2\text{CH}_2\text{OH}$ ) by Hollis et al. (2000, 2002) which emphasize that large biomolecules are common constituents of interstellar clouds.

The first glycine spectrum observed in the laboratory was a high energy conformer (later designated conformer II), and its assignment was reported contemporaneously by two independent groups (Brown et al. 1978; and Suenram & Lovas 1978). Later, Suenram & Lovas (1980) analyzed conformer I glycine. Lovas et al. (1995) showed that conformer I glycine is  $705\text{ cm}^{-1}$  (1012 K) lower in energy than conformer II glycine, and that the dipole moments are  $\mu_a = 0.911\text{ D}$  and  $\mu_b = 0.607\text{ D}$  for conformer I and  $\mu_a = 5.372\text{ D}$  and  $\mu_b = 0.93\text{ D}$  for conformer II. (While at least six glycine conformers are possible in theory, only conformers I and II have ever been observed in the laboratory.) Since molecular line intensity is proportional to the square of the dipole moment, glycine *a*-type transitions are the more likely to be detected in interstellar clouds. Conformer II spectra dominate conformer I spectra in a laboratory absorption cell because of its larger dipole moment and the high sample cell wall temperature ( $\geq 450\text{ K}$ ). The expected line intensities of the two conformers equalize at  $\sim 285\text{ K}$ . Thus, if the temperature of an interstellar molecular source is  $\leq 100\text{ K}$  (e.g., OMC-1), then conformer I glycine *a*-type transitions would be the candidate lines most likely to be detected.

Following the successful laboratory measurements, searches for interstellar glycine have been conducted by various groups (Brown et al. 1979; Hollis et al. 1980; Snyder et al. 1983; Beralis et al. 1985; Guelin & Cernicharo 1989; Combes, Rieu, & Wlodarczak 1996; Snyder 1997; Ceccarelli et al. 2000). Combes et al. (1996) conducted the most sensitive previous search for glycine using the IRAM 30-m telescope at 3 mm with a 24" beam size; at the same time, they also searched at 1 and 2 mm with beam sizes of 13" and 19", respectively. We proposed to conduct a glycine search with the NRAO<sup>8</sup> Very Large Array

---

<sup>8</sup>The National Radio Astronomy Observatory is a facility of the National Science Foundation operated under cooperative agreement by Associated Universities, Inc.

---

(VLA) for a number of reasons: First and foremost, interstellar glycine may have a spatial scale of one or two arc seconds; such a scale size can only be detected with a sensitive

interferometer because beam dilution would plague a single-element antenna. Second, telescope sensitivity is proportional to collecting area and the VLA has ~20 times the collecting area of the IRAM 30-m telescope. Third, all VLA antennas have been recently equipped with receivers at Q-band (~7 mm) which is the only VLA operating band with enough tunable range (40-50 GHz) in which several likely transitions of glycine could be observed. Fourth, the VLA acts as a spatial filter which resolves out emission from small molecules that form in extended envelopes, thereby reducing the line confusion level to make it possible to detect larger molecules that are prone to survive in embedded compact sources. Fifth, different complex molecules often have very different spatial distributions; such spatial association can be used to help sort through the spectral line confusion.

This work reports the results of a deep search of the low temperature environment of OMC-1 with the VLA for four conformer I glycine *a*-type transitions in the Q-band range. This is the first Q-band glycine search to be conducted with an interferometer.

## 2. OBSERVATIONS

Simultaneous Q-band observations of glycine and silicon monoxide or methyl formate and formic acid were conducted toward OMC-1 with the VLA in 2001 September (DnC configuration) and 2001 December (D configuration) at epochs and scheduled observing time specified in Table 1 cols. (1) and (2), respectively. The J2000 phase center for all observations was  $\alpha = 5^{\text{h}}35^{\text{m}}14^{\text{s}}.25$ ,  $\delta = -5^{\circ}22'35''.5$ , which is midway between the Orion hot core and the OMC-1 formic acid positions given in Liu et al. (2002). Moreover, the phase center position is within ~1" of the pointing position used by Combes et al. (1996). The VLA primary beam is  $\approx 45/\nu(\text{GHz})$  arcminutes -- thus, the nominal primary beam for our observations was ~1'. The VLA correlator was operated in the Four IF normal mode, which yields 32 spectral channels with a spacing of 195.313 kHz (~1.36 km s<sup>-1</sup>) for both left and right circular polarizations. An assumed LSR source velocity of +8.0 km s<sup>-1</sup> was centered in the resulting 6.25 MHz (~43.5 km s<sup>-1</sup>) bandpass. Observed molecules and

bandpass center frequencies are shown in Table 1 cols. (3) and (4). Table 2 lists the glycine transition parameters: the rotational quantum numbers (col. 1); the transition rest frequency (col. 2); the upper energy level  $E_u$  (col. 3) in Kelvins; and the transition line strength  $S$  (col. 4).

Quasars 0607-085 and 3C84 were used as the phase and bandpass calibrators, respectively. The absolute flux density scale was determined from observations of 3C286 (Sep 16 through Dec 20) or 3C48 (Dec 23 and 26) whose 43 GHz flux density is 1.44 Jy or 0.52 Jy, respectively, as given by the SETJY routine in AIPS. The latest antenna gain curves were applied using the FIXQGAIN procedure (S. Meyers, private communication). The bootstrapped flux densities of 0607-085 and 3C84 at each observing epoch (Table 1 cols. 5 and 6, respectively) show satisfactory repeatability and are in good agreement with NRAO monitoring results. However, on the dates where 0607-085 and 3C84 fluxes appeared systematically low or high (see Table 1), a median flux value of 1.63 Jy is adopted for 0607-085.

The antenna gains were derived from 0607-085 observations at 10-30 min intervals and applied to the data using standard AIPS routines. Phase self-calibration on vibrationally excited SiO maser emission (Table 1) was used to derive fast timescale (5s) atmospheric phase variations and the solutions were applied to the corresponding glycine line data. This correction was not applicable for the methyl formate and formic acid data. The extensive set of SiO observations will be the subject of a future paper.

Continuum subtraction was performed using the UVLIN routine. Continuum subtracted data cubes of total intensity emission were created by averaging the right and left circularly polarized visibilities. The rms noise levels in each plane of a continuum subtracted cube range from 15 to 50% above the theoretical noise limit, which is reasonable for a low declination source (maximum elevation was  $\sim 50^\circ$ ). The naturally weighted synthesized beams resulting from DnC and D configurations were  $\sim 1.9'' \times 1.6''$  and  $\sim 2.9'' \times 1.9''$ , respectively.

### 3. RESULTS

During the 2001 September observations, we devoted each track to one transition of glycine (as shown in Table 1) except the  $7_{07} - 6_{06}$  transition which was observed twice because it has the largest line strength (see Table 2, col. 4). Based on BIMA Array formic acid observations (Liu et al. 2002), our search probed regions of peak formic acid emission which are found predominantly along the OMC-1 compact ridge at  $+8.0 \text{ km s}^{-1}$  LSR velocity. In 2001 December, we observed the  $7_{07} - 6_{06}$  glycine transition in three tracks with a four channel frequency shift. Table 2 col. (5) summarizes the emission limits provided by our glycine search. Two remaining tracks in 2001 December were used to detect the  $2_{02} - 1_{01}$  transition of formic acid and the  $4_{14} - 3_{13}$  transition of methyl formate. Formic acid was chosen since both it and glycine share the structural carboxyl group ( $\text{COOH}$ ), which is seemingly rare in interstellar clouds. Because of this structural similarity, it may well be that both species share common formation pathways. Further, one would expect to find both species in spatial proximity, but not necessarily spatially coincident, if the formic acid is a precursor which is used up in the process of glycine formation. Methyl formate was chosen because it is a ubiquitous interstellar isomer of both acetic acid and glycolaldehyde, and its 8-atom size is more comparable to 10-atom glycine. Table 2 cols. (5), (6), and (7) summarize the formic acid and methyl formate emission features detected.

Table 2 lists the beam-averaged column densities  $N_T$  (cols. 9 and 10) for formic acid and methyl formate and upper limits for glycine. These column densities were calculated from the following expression (Liu, Mehringer, & Snyder 2001) which assumes optically thin LTE conditions and does not account for possible beam dilution:

$$N_T = 2.17 \times 10^{20} \frac{\Delta I \Delta V Q_{\text{ROT}} \exp(E_u/T_{\text{ROT}})}{\theta_a \theta_b v^3 S \mu^2}. \quad (5)$$

In equation (5),  $N_T$  is in  $\text{cm}^{-2}$ ;  $\nu$  is the rest frequency in GHz;  $E_u$  is the upper rotational level in K;  $S$  is the line strength;  $\mu$  is the dipole moment in debye (i.e., 0.911 D);  $\Delta I$  is the peak line intensity in  $\text{Jy beam}^{-1}$ ;  $\Delta V$  is the FWHM linewidth in  $\text{km s}^{-1}$ ; the product  $\theta_a \theta_b$  is the Gaussian FWHM dimensions of the synthesized beam in  $\text{arcsec}^2$  (Table 2, col. 8);  $Q_{\text{ROT}}$ , the dimensionless rotational partition function, is  $15.6 \times T_{\text{ROT}}^{1.5}$ ,  $1.7 \times T_{\text{ROT}}^{1.5}$ , or  $12.45 \times T_{\text{ROT}}^{1.5}$  for glycine, formic acid, or methyl formate, respectively (e.g., Gordy and Cook 1984); and  $T_{\text{ROT}}$ , the rotational temperature, is assumed to be either 43 K, a value based on a rotational diagram method for formic acid (Liu et al. 2002), or 100 K, a value approximately representative of other molecular species toward the Orion compact ridge (e.g., Wright et al. 1996).

Figures 1 and 2 show contour maps and spectra, respectively, of the A and E symmetry states of the  $4_{14} - 3_{13}$  transition of methyl formate. Positions of continuum source I and the infrared BN object (e.g., Menten & Reid 1995) are provided in Figure 1 and subsequent spatial imaging figures for reference. Figures 1 and 2 of methyl formate demonstrate that the A and E symmetry lines possess nearly identical spectra and nearly the same spatial morphology as expected for high signal-to-noise data (cf. Figure 1 panels d and e of Minh et al. 1993).

Figures 3 and 4 show a contour map and spectrum, respectively, of the  $2_{02} - 1_{01}$  transition of formic acid that results from a convolution with a 6" circular gaussian to enhance the extended structure of this weak emission. As a result, formic acid is convincingly detected at the  $\sim 20 \text{ mJy beam}^{-1}$  level for this extended beam size. For a naturally weighted beam size, as shown in Table 2, formic acid has a peak intensity of  $\sim 5 \text{ mJy beam}^{-1}$ . Liu et al. (2002) have shown that methyl formate and formic acid in OMC-1 are not spatially coincident. In Figure 5, methyl formate emission is between source I and the formic acid source. The position of continuum source I marks the centroid of SiO maser emission and is, therefore, the source of molecular outflow. Liu et al. (2002) suggest the formic acid source is located in a layer which delineates the shock interaction as the



outflow plows into the ambient quiescent gas. Thus, in this scenario, methyl formate would represent older, post-shock gas.

#### 4. DISCUSSION

The detection and spatial imaging of the  $4_{14} - 3_{13}$  A and E transitions of methyl formate ( $\text{HCOOCH}_3$ ) and the  $2_{02} - 1_{01}$  transition of formic acid ( $\text{HCOOH}$ ) in OMC-1 demonstrate that these weak molecular emission lines originate in compact sources. Since formic acid is a possible precursor to glycine (as shown in equation 4), our glycine limits and formic acid results provide a constraint on this potential formation chemistry route for glycine in compact sources of emission toward OMC-1. For example, comparing column density results (Table 2 col. 9) for the same beam size (Table 2 col. 8), the abundance of glycine is less than or equal to the formic acid abundance in OMC-1.

The most severe upper limit recently quoted (e.g. Ehrenfreund & Menten 2002) on the glycine-to-molecular-hydrogen fractional abundance ratio ( $X_{\text{Gly}}$ ) toward interstellar sources is of order  $10^{-10}$ , which is based on observations with the IRAM 30m telescope (Combes et al. 1996). We will show that this value is optimistic. Any such quoted limit must be carefully qualified. First, conversion of a measured upper limit for a line flux to an upper limit for a beam-averaged column density depends on several assumptions. Typically, for upper limits, one assumes that the optical depth is small, LTE conditions at a known temperature prevail, and possible beam dilution is ignored. This is what we have done in equation (5) and Combes et al. (1996) have done in their work. Second, forming abundance ratios implicitly assumes that the two molecules are spatially coincident. Even with this assumption, the abundance ratios are model dependent unless both measurements were made with the same beam. For the same total number of molecules in the source, the beam-averaged column densities derived from observations that reach the same flux-sensitivity with two different beams will be different. If the source is small relative to the beam, there

will be beam-dilution, but, if the source is large relative to the beam, flux will be missed because the instrument is only sensitive to beam-sized spatial scales.

Beam dilution must be addressed when comparing observations where telescope beams differ significantly (e.g., the VLA and IRAM 30m telescope) by computing a beam filling factor (B), a fraction  $\leq 1$  which is applied by division into the observed emission intensity (equivalently the column density as per equation 5 which assumes  $B=1$ ). For a circular gaussian telescope beam size ( $\theta_b$ ) centered on the peak of a circular gaussian source of size ( $\theta_s$ ), the resulting simple convolution yields a beam filling factor (B) given by (e.g., see equation 28 of Ulich & Haas 1976):

$$B = \frac{\theta_s^2}{\theta_b^2 + \theta_s^2} \quad (6)$$

For an infinitely extended source, B approaches unity. If the source size is very small compared to the telescope beam, B approaches zero. A source size must be assumed, estimated or modeled a priori so that the actual value of B can be determined for each telescope beam involved. Thus, in the following, we compare VLA and IRAM 30m  $X_{\text{Gly}}$  ratio limits that result from taking into account source size.

Our VLA experiment is the first sensitive search for glycine in OMC-1 sources that have angular sizes on the order of  $\sim 2''$ . We consider three possible glycine source sizes in OMC-1 when computing  $X_{\text{Gly}}$  ratios. Since glycine contains an amine group ( $\text{NH}_2$ ), we choose nitrogen bearing molecules that have been observed with an interferometer to obtain physically meaningful source sizes. From Wright et al. (1996, figure 1), we select ethyl cyanide ( $\text{CH}_3\text{CH}_2\text{CN}$ ), a nine-atom molecule that rivals the size of glycine; from Wilson et al. (2000, figure 2), we select ammonia ( $\text{NH}_3$ ), a well-known hot core constituent of OMC-1; and, finally, we assume a true source size equal to VLA beam size. Table 3 summarizes the apparent size (col. 1), the imaging beam size (col. 2), and the true size (col. 3) for these three selections. True sizes (s) were deconvolved from the observed apparent sizes (obs) in the circular beam (b) approximation (e.g., see equation 8.15 of Rohlfs & Wilson 2000):

$$\theta_{\text{obs}}^2 = \theta_s^2 + \theta_b^2 \quad (7)$$

To estimate the molecular hydrogen column densities needed to form  $X_{\text{Gly}}$  ratios, we follow Wright et al. (1996) who use observations of optically thin 3 mm dust emission in OMC-1. Molecular hydrogen column density determinations from dust emission are not straightforward and have an order of magnitude uncertainty (Wright et al. 1996). For the OMC-1 compact ridge which was observed with a beam size of 7" x 5", Wright et al. (1996, table 4) derived an observed molecular hydrogen beam-averaged column density of  $\sim 2 \times 10^{23} \text{ cm}^{-2}$ .

VLA  $3\sigma$  upper limits to the glycine beam-averaged column density toward the compact ridge in OMC-1 (Table 2 cols. 9 and 10) assume a beam filling factor of unity and are a function of the synthesized beam size used, the rotational temperatures assumed, and the  $3\sigma$  noise levels estimated in the final images. The  $7_{07} - 6_{06}$  transition was observed with more integration time than other glycine transitions, and therefore provides the best constraint on glycine total column density for a naturally weighted VLA beam size of 2.3" x 1.7" (see Table 2). The rotational temperature of glycine is problematical in OMC-1 where characteristic temperatures typically range from 50 to 100 K (e.g., see Combes et al. 1996). However, our VLA observations would be more sensitive to hotter compact core emission, and therefore we use the hotter Table 2 column density  $3\sigma$  limit (i.e.,  $< 4.64 \times 10^{15} \text{ cm}^{-2}$ ) as characteristic of the transition of glycine for the 2.3" x 1.7" VLA beam case. The IRAM 30m telescope was used at 3 mm (FWHM = 24") to obtain a  $1\sigma$  limit for a beam-averaged glycine column density of  $< 5 \times 10^{13} \text{ cm}^{-2}$  assuming a temperature of 100 K (Combes et al. 1996; N.-Q. Rieu, private communication). For comparison of results between the two telescopes, we use the  $3\sigma$  glycine beam-averaged column density upper limits of  $< 4.64 \times 10^{15} \text{ cm}^{-2}$  and  $< 1.5 \times 10^{14} \text{ cm}^{-2}$  for the VLA and IRAM 30m telescope, respectively. When forming  $X_{\text{Gly}}$  from column density measurements or upper limits obtained with different telescope beams ( $\Omega$ ), one must multiply the beam-averaged column density ratio by the inverse of the ratio of beam filling factors:

$$X_{\text{Gly}} = \frac{N_{\text{T}}(\text{Gly})}{N_{\text{T}}(\text{H}_2)} \frac{B(\Omega(\text{H}_2))}{B(\Omega(\text{Gly}))} \quad (8)$$

As per equation (8), beam filling factor ratios and  $X_{\text{Gly}}$  ratio limits are shown in Table 3 cols. (4) and (5), respectively, for the three source models considered for each telescope (i.e., either the VLA or the IRAM 30m as shown in col. 6).

Table 3 shows that for decreasing source sizes, the  $X_{\text{Gly}}$  ratio limits range from  $< 1.6 \times 10^{-8}$  to  $< 4.7 \times 10^{-9}$  for the VLA while the same limits range from  $< 4.6 \times 10^{-9}$  to  $< 1.1 \times 10^{-8}$  for the IRAM 30m. Alternatively stated: For a source size like that of ethyl cyanide, the IRAM 30m telescope produces an  $X_{\text{Gly}}$  ratio limit  $\sim 3.5$  times more severe than the VLA; on the other hand, for source sizes like that of ammonia and the VLA beam itself, the VLA produces  $X_{\text{Gly}}$  ratio limits of  $\sim 1.5$  and  $\sim 2.3$  times, respectively, more severe than the IRAM 30m.

It is emphasized that Table 3 limits are based on conformer I glycine observations only and at temperatures  $\leq 100$  K. Under more extreme hot core conditions (e.g., 300 to 600 K), the prevalent form of glycine may well be conformer II (see discussion in § 1).

## 5. SUMMARY

We conducted a deep Q-band search with the VLA toward OMC-1 for conformer I glycine in four rotational transitions: the  $6_{15} - 5_{14}$ ,  $6_{24} - 5_{23}$ ,  $7_{17} - 6_{16}$ , and  $7_{07} - 6_{06}$ . No glycine emission features were detected, suggesting that either conformer I glycine is below our detection limit, or is more spatially extended than other large molecules in OMC-1. Alternatively, glycine may be primarily in its high energy form (conformer II). For future OMC-1 searches, we found that the four glycine Q-band transitions we attempted to observe appear clear of contaminating line emission from other species. We carefully discussed the necessity to account for the sizes of the beams used in all of the observations

-- both glycine and molecular hydrogen. Our measurements were used to determine upper limits on the total column density of glycine toward OMC-1. These results yield  $X_{\text{Gly}}$  ratio limits ranging from  $< 1.6 \times 10^{-8}$  to  $< 4.7 \times 10^{-9}$  for source sizes of  $12.1'' \times 5.9''$  to  $2.3'' \times 1.7''$ , respectively. We conclude that the VLA conformer I  $X_{\text{Gly}}$  ratio limits in OMC-1 are comparable to the previous IRAM result -- somewhat better or worse depending on the assumed size of the glycine source -- and in none of the cases have  $X_{\text{Gly}}$  ratio limits for either telescope attained a value as low as  $10^{-10}$ . Furthermore, the VLA results apply to the entire  $\sim 1'$  primary beam while being sensitive to an areal spatial scale  $\sim 150$  times smaller than the  $24''$  beam of the IRAM single-element telescope. We were able to detect and spatially image the  $4_{14} - 3_{13}$  A and E transitions of methyl formate and also the  $2_{02} - 1_{01}$  transition of formic acid. These positive results demonstrate the viability of the VLA as a sensitive search instrument for weak molecular lines of biological importance.

We appreciate the VLA scheduling efforts of Barry Clark on our behalf, the suggestion of an anonymous reviewer that we compare VLA and IRAM results for a number of source sizes, and clarifying information provided by Nguyen-Quang Rieu regarding previous glycine limit results with the IRAM 30m telescope. J.M.H. and J.A.P. received support from NASA RTOP 344-02-03-01. L.E.S. and F.J.L. received support from the Laboratory of Astronomical Imaging at the University of Illinois, and NSF grant AST 99-81363. P.P. received support from NASA grant NAG5-8708. S.-Y. Liu received support from NSF grant AST 99-81546.

TABLE 1  
Summary of Observational Parameters

	Observing	1st Line	2nd Line	0607-085	3C84
Date	Time	Frequency	Frequency	Flux	Flux
(2001) (1)	(hrs) (2)	(MHz) (3)	(MHz) (4)	(Jy) <sup>a,b</sup> (5)	(Jy) <sup>a,b</sup> (6)
<hr/>					
		<u>NH<sub>2</sub>CH<sub>2</sub>COOH<sup>c</sup></u>	<u>SiO (J = 1 – 0)<sup>d</sup></u>		
Sep 16	5.5	43183.651	43122.080 (v=1)	1.55(2)	6.87(16)
18	7.0	43753.841	43423.858 (v=0)	1.88(11)	8.52(50)
27	5.0	42985.223	43122.080 (v=1)	1.64(3)	7.31(12)
28	6.0	42637.789	42820.587 (v=2)	1.62(3)	7.30(15)
29	6.5	43753.841	43423.858 (v=0)	1.64(2)	7.36(12)
Dec 07	5.0	43754.621	43423.858 (v=0)	1.48(2)	6.99(18)
10	10.0	43754.621	43423.858 (v=0)	1.66(2)	9.93(17)
20	5.0	43754.621	43423.858 (v=0)	1.06(2)	4.92(15)
		<u>HCOOCH<sub>3</sub><sup>e</sup></u>	<u>HCOOH<sup>e</sup></u>		
23	3.5	45396.636	44911.75	...	...
26	4.0	45396.636	44911.75	0.95(2)	4.05(14)

<sup>a</sup>Flux density is the average at the two observing frequencies. A 1.63 Jy flux density for 0607-085 was used in calibration procedures on Sep 18, Dec 20, 23, and 26 (see § 2).

<sup>b</sup>Uncertainties in parentheses refer to the least significant digit and are 1 $\sigma$  values.

<sup>c</sup>September glycine observational frequencies are line rest frequencies as shown in Table 2. December glycine observational frequencies are shifted higher approximately four channel spacings (see § 3).

<sup>d</sup>Rest frequencies from Lovas (1992).

<sup>e</sup>Rest frequencies shown in Table 2. Methyl formate is approximately centered between the rest frequencies for the A and E symmetry states.

TABLE 2

Summary of the Spectral Line Search Toward OMC-1

Transition $J'_{K-K+} - J''_{K-K+}$ (1)	Frequency (MHz) (2) <sup>a</sup>	$E_u$ (K) (3)	S (4)	$\Delta I(\text{peak})$ (mJy beam <sup>-1</sup> ) (5) <sup>a,b</sup>	$\Delta V$ (km s <sup>-1</sup> ) (6) <sup>a,b</sup>	$V_{\text{LSR}}$ (km s <sup>-1</sup> ) (7) <sup>a</sup>	$\theta_a \times \theta_b$ (" x ") (8)	$N_T \times 10^{-14}$ $T_{\text{ROT}}=43 \text{ K}$ (cm <sup>-2</sup> ) (9) <sup>a,c</sup>	$N_T \times 10^{-14}$ $T_{\text{ROT}}=100 \text{ K}$ (cm <sup>-2</sup> ) (10) <sup>a,c</sup>
Glycine <sup>d</sup> :									
6 <sub>15</sub> - 5 <sub>14</sub>	42637.789(6)	7.574	5.774	<0.9	3.9	...	1.9x1.6	<35.4	<114.0
6 <sub>24</sub> - 5 <sub>23</sub>	42985.223(30)	8.420	5.350	<0.9	3.9	...	1.9x1.6	<38.0	<121.0
7 <sub>17</sub> - 6 <sub>16</sub>	43183.651(25)	8.700	6.818	<0.9	3.9	...	1.9x1.7	<27.9	< 88.1
7 <sub>07</sub> - 6 <sub>06</sub>	43753.841(28)	8.657	6.851	<0.6	3.9	...	2.3x1.7	<14.7	< 46.4
				<3.0	3.9	...	6.0x6.0	<8.0	< 25.2
Formic Acid <sup>e</sup> :									
2 <sub>02</sub> - 1 <sub>01</sub>	44911.75(5)	3.233	2.000	5.0(3)	3.9(7)	8.0(7)	3.0x1.6	13.1(32)	...
				20.0(10)	3.9(7)	8.0(7)	6.0x6.0	7.0(16)	...
Methyl Formate <sup>f</sup> :									
4 <sub>14</sub> - 3 <sub>13</sub> E	45395.775(16)	6.146	9.947	85.8(4)	3.9(7)	7.7(7)	2.9x1.5	274(51)	894(166)
4 <sub>14</sub> - 3 <sub>13</sub> A	45397.394(16)	6.128	9.947	84.4(4)	3.9(7)	7.7(7)	2.9x1.5	269(50)	879(163)

<sup>a</sup>Uncertainties in parentheses refer to the least significant digit(s) and are 2 $\sigma$  values for col. (2) and 1 $\sigma$  estimates

for cols. (5), (6), (7), (9) and (10).

<sup>b</sup>Glycine limits in cols. (5), (9), and (10) are 3 $\sigma$  estimates and glycine linewidths assumed in col (6) are based on the nominal values observed for formic acid and methyl formate.<sup>c</sup>Abundance values or limits were computed using equation (6) with  $T_{\text{ROT}} = 43 \text{ K}$  (col. 9) or 100 K (col. 10) as justified in § 3.<sup>d</sup>Dipole moment  $\mu_a = 0.911 \text{ D}$  (Lovas et al. 1995); rest frequencies calculated in this work.<sup>e</sup>Dipole moment  $\mu_a = 1.391 \text{ D}$  (Kim, Keller, & Gwinn 1962); rest frequencies (Willmot et al. 1980).<sup>f</sup>Dipole moment  $\mu_a = 1.63 \text{ D}$  (Curl 1959); rest frequencies (Oesterling et al. 1999).

TABLE 3  
Glycine-to-Molecular-Hydrogen Abundance Ratio  $3\sigma$  Limits for Three Source Models

Apparent Source (" x ") (1)	Imaging Beam (" x ") (2)	True Source (" x ") (3)	$\frac{B(\Omega(\text{H}_2))}{B(\Omega(\text{Gly}))}$ (4) <sup>a</sup>	$X_{\text{Gly}}$ (5)	Telescope (6)
14 x 7.7 (CH <sub>3</sub> CH <sub>2</sub> CN map)	7 x 5	12.1 x 5.9	6.1445 0.6995	<4.6 x 10 <sup>-9</sup> <1.6 x 10 <sup>-8</sup>	IRAM VLA
4.9 x 1.9 (NH <sub>3</sub> map)	1.3 x 0.9	4.7 x 1.7	13.2146 0.2825	<9.9 x 10 <sup>-9</sup> <6.6 x 10 <sup>-9</sup>	IRAM VLA
N/A	N/A	2.3 x 1.7 (assumed)	14.9077 0.2010	<1.1 x 10 <sup>-8</sup> <4.7 x 10 <sup>-9</sup>	IRAM VLA

<sup>a</sup>The ratio of the beam filling factor of Wright et al. (1996) -- who used a 7" x 5" beam to obtain an observed  $N_{\text{T}}(\text{H}_2) = 2 \times 10^{23} \text{ cm}^{-2}$  -- to the beam filling factor of either the 24" circular beam of the IRAM 30m or the 2.3" x 1.7" gaussian VLA beam used to observe glycine (see § 4 text and equation 8)



## REFERENCES

- Beralis, I.I., Winnewisser, G., Krasnov, V.V., & Sorochenko, R.L. 1985, *Sov. Astron. Lett.*, 11, 251
- Bernstein, M.P., Dworkin, J.P., Sandford, S.A., Cooper, G.W., & Allamandola, L.J. 2002, *Nature*, 416, 401
- Brown, R.D., Godfrey, P.D., Storey, J.W.V., & Bassez, M.-P. 1978, *J.C.S. Chem. Comm.*, p. 547
- Brown, R.D., Godfrey, P.D., Storey, J.W.V., Bassez, M.-P., Robinson, B.J., Batchelor, R.A., McCulloch, M.G., Rydbeck, O.E.A., & Hjalmarson, A.G. 1979, *MNRAS*, 186, 5P
- Ceccarelli, C., Loinard, L., Castets, A., Faure, A., & Lefloch, B. 2000, *A&A*, 362, 1122
- Charnley, S.B., Ehrenfreund, P., & Kuan, Y.-K. 2001, *Spectrochimica Acta Part A*, 57, 685
- Combes, F., Nguyen-Q-Rieu, & Wlodarczak, G. 1996, *A&A*, 308, 618
- Curl, R.F., Jr., 1959, *J.Chem.Phys.*, 30, 1529
- Ehrenfreund, P., & Menten, K.M. 2002, in *Astrobiology: The Quest for the Conditions of Life*, eds. G. Horneck and C. Baumstark-Khan (Berlin: Springer-Verlag), 7
- Gordy, W. & Cook, R.L. 1984, in *Microwave Molecular Spectra*, (New York: Wiley-Interscience), p. 58
- Guelin, M., & Cernicharo, J. 1989, in *The Physics and Chemistry of Interstellar Molecular Clouds*, eds. G. Winnewisser and J.T. Armstrong, (Berlin: Springer-Verlag), 337
- Hollis, J.M., Lovas, F.J., & Jewell, P.R. 2000, *ApJ*, 540, L107
- Hollis, J.M., Snyder, L.E., Suenram, R.D., & Lovas, F.J. 1980, *ApJ*, 241, 1001
- Hollis, J.M., Lovas, F.J., Jewell, P.R., Coudert, L.H. 2002, *ApJ*, 571, L59
- Kim, H., Keller, R., & Gwinn, W.D. 1962, *J.Chem.Phys.*, 37, 2748
- Kissel, J., & Krueger, F.R. 1987, *Nature*, 326, 755
- Liu, S.-Y., Girart, J.M., Remijan, A., & Snyder, L.E. 2002, *ApJ*, 576, 255

- Liu, S.-Y., Mehringer, D.M., & Snyder, L.E. 2001, *ApJ*, 552, 654
- Lovas, F. J. 1992, *J. Phys. Chem. Ref. Data*, 21, 181
- Lovas, F. J., Kawashima, Y., Grabow, J.-U., Suenram, R. D., Fraser, G. T., & Hirota, E. 1995, *ApJ*, 455, L201
- Mehringer, D.M., Snyder, L.E., Miao, Y., & Lovas, F.J. 1997, *ApJ*, 480, L71
- Menten, K. M., & Reid, M.J. 1995, *ApJ*, 445, L157
- Minh, Y. C., Ohishi, M., Roh, D. G., Ishiguro, M., & Irvine, W. M. 1993, *ApJ*, 411, 773
- Muñoz Caro, G.M., Meierhenrich, U.J., Schutte, W.A., Barbier, B., Segovia, A.A., Rosenbauer, H., Thiemann, W.H.-P., Brack, A., & Greenberg, J.M., 2002, *Nature*, 416, 403
- Oesterling, L.C., Albert, S., De Lucia, F.C., Sastry, K.V.L.N., & Herbst, E. 1999, *ApJ*, 521, 255
- Remijan, A.J., Snyder, L.E., Liu, S.-Y., Mehringer, D.M., & Kuan, Y.-J. 2002, *ApJ*, 576, 264
- Rohlfs, K., & Wilson, T.L. 2000, in *Tools of Radio Astronomy*, (3 rd ed.; Berlin: Springer-Verlag), 192
- Snyder, L.E. 1997, *Orig. Life & Evol. Biosph.*, 27, 115
- Snyder, L.E., Hollis, J.M., Suenram, R.D., Lovas, F.J., Brown, L.W., & Buhl, D. 1983 *ApJ*, 286, 123
- Sorrell, W.H. 2001, *ApJ*, 555, L129
- Suenram, R.D., & Lovas, F.J. 1978, *J.Molec. Spectrosc.*, 72, 372
- Suenram, R.D., & Lovas, F.J. 1980, *J.Am.Chem.Soc.*, 102, 7180
- Ulich, B.L., & Haas, R.W., 1976, *ApJS*, 30, 247
- Willemot, E., Dangoisse, D., Monnanteuil, N., & Bellet, J. 1980, *J. Phys. Chem. Ref. Data*, 9, 59
- Wilson, T.L., Gaume, R.A., Gensheimer, P., & Johnston, K.J. 2000, *ApJ*, 538, 665
- Wright, M.C.H., Plambeck, R.L., & Wilner, D.J. 1996, *ApJ*, 469, 216

# FIGURE CAPTIONS

Fig. 1 -- Contour maps of the A and E symmetry states of the  $4_{14} - 3_{13}$  transition of methyl formate toward OMC-1. The maps were made directly from continuum subtracted u,v visibilities; data from spectral channels 10 through 13 (18 through 21) were Hanning smoothed and summed to produce the E symmetry state (A symmetry state) contour plots in panel a (panel b). Comparison of panels a and b verify expectations that transitions of a given molecule with the same excitation parameters (i.e., line strength, energy level, dipole moment, etc.) should be morphologically identical. The  $2.90'' \times 1.52''$  naturally weighted beam size is shown in the lower left of each panel. Contour intervals are -3.5, 3.5, 7, 10.5, 14, 17.5, 21, 24.5, 28, 35, 42, 49, and 56 mJy beam<sup>-1</sup> with peak fluxes of 60.2 (58.7) mJy beam<sup>-1</sup> in panel a (panel b). In both panels, the 3.5 mJy beam<sup>-1</sup> contour level corresponds to a  $3\sigma$  detection level.

Fig. 2 -- Spectrum of the  $4_{14} - 3_{13}$  transition of methyl formate showing A and E symmetry states toward OMC-1 at 195 kHz channel spacing. Spectral channels 4 through 28 are shown. Transition quantum numbers are shown in the upper right. The frequency axis and the LSR velocity axis reflect the LSR velocity of  $\sim 8.0$  km s<sup>-1</sup> assumed for this source position at a rest frequency of 45396.636 MHz (i.e., approximately midway between the A and E features). This spectrum was taken at the most intense position shown in Figure 1 with a beam size of  $2.90'' \times 1.52''$ .

Fig. 3 -- Contour map of the  $2_{02} - 1_{01}$  transition of formic acid toward OMC-1. A map was made directly from continuum subtracted u,v visibilities and convolved with a 6" x 6" circular gaussian, whose size is shown in the lower left. The convolution was necessary to recover flux from this obviously extended source. Data from spectral channels 15 through 17 were Hanning smoothed and summed to produce the contour plot. Contour intervals are -6, -3, 3, 6, 9, and 12 mJy beam<sup>-1</sup> with a peak flux of 13.6 mJy beam<sup>-1</sup>. The 3 mJy beam<sup>-1</sup> contour level corresponds to a 1 $\sigma$  detection level.

Fig. 4-- Spectrum of the  $2_{02} - 1_{01}$  transition of formic acid toward OMC-1 at 195 kHz channel spacing. Spectral channels 4 through 28 are shown. Transition quantum numbers are shown in the upper right. The frequency axis and the LSR velocity axis reflect the LSR velocity of  $\sim 8.0$  km s<sup>-1</sup> assumed for this source position at a line rest frequency of 44911.75 MHz. This spectrum was taken at the most intense position shown in Figure 3 with a 6.0" circular synthesized beam.

Fig. 5 -- Contour map of the average of A and E symmetry states for the  $4_{14} - 3_{13}$  transition of methyl formate toward OMC-1 superimposed on a gray scale intensity map of the  $2_{02} - 1_{01}$  transition of formic acid. See Figure 1 caption which describes the methyl formate map production and similarly Figure 3 caption regarding formic acid map production. Contour intervals for the methyl formate are -4, 4, 8, 12, 16, 20, 24, 28, 32, 40, 48, 56, and 63 mJy beam<sup>-1</sup> with a peak intensity of 63.8 mJy beam<sup>-1</sup>. The 2.90" x 1.52" naturally weighted beam size for the methyl formate is shown in the lower left.

Fig. 1a

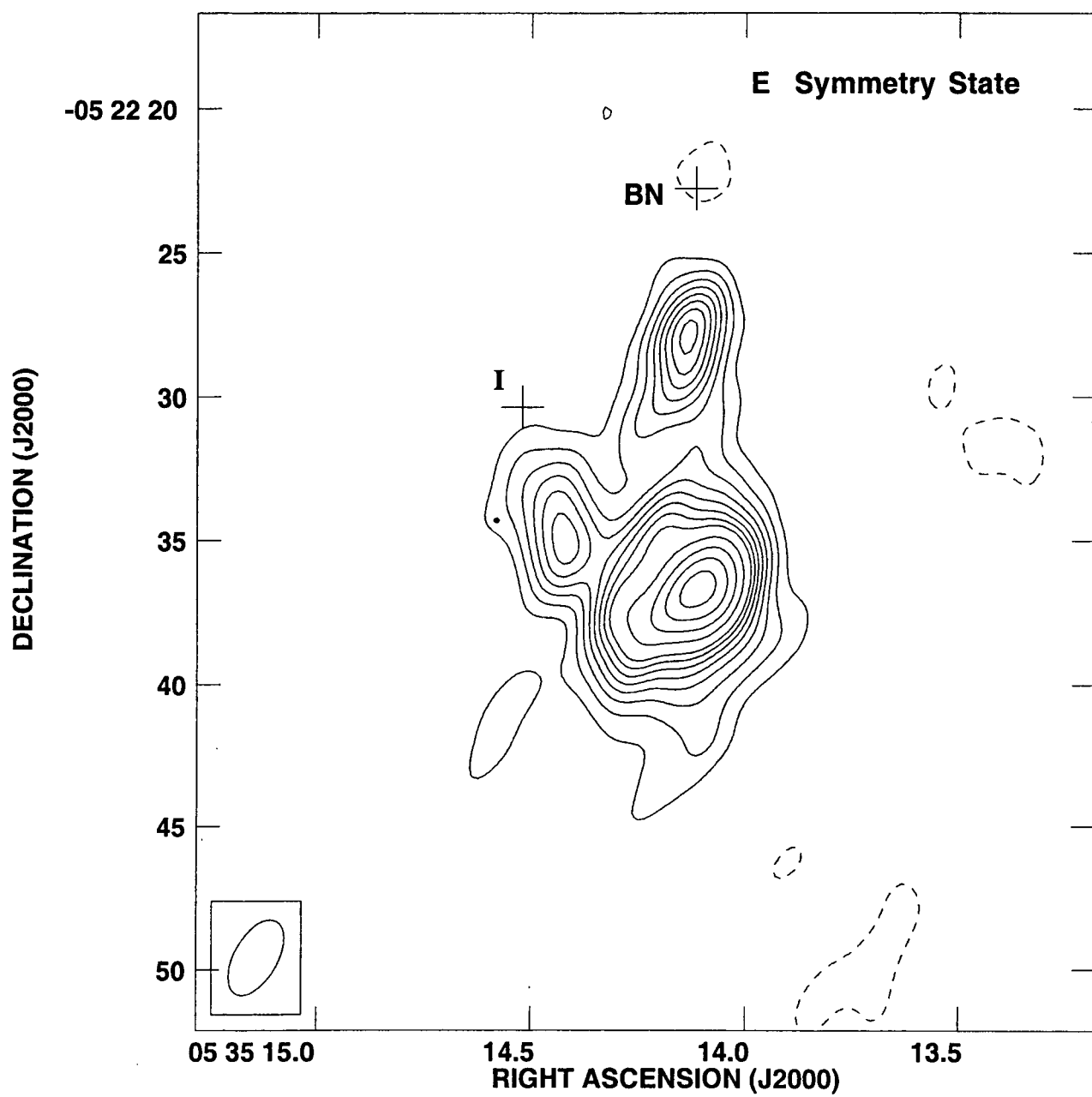


Fig. 1b

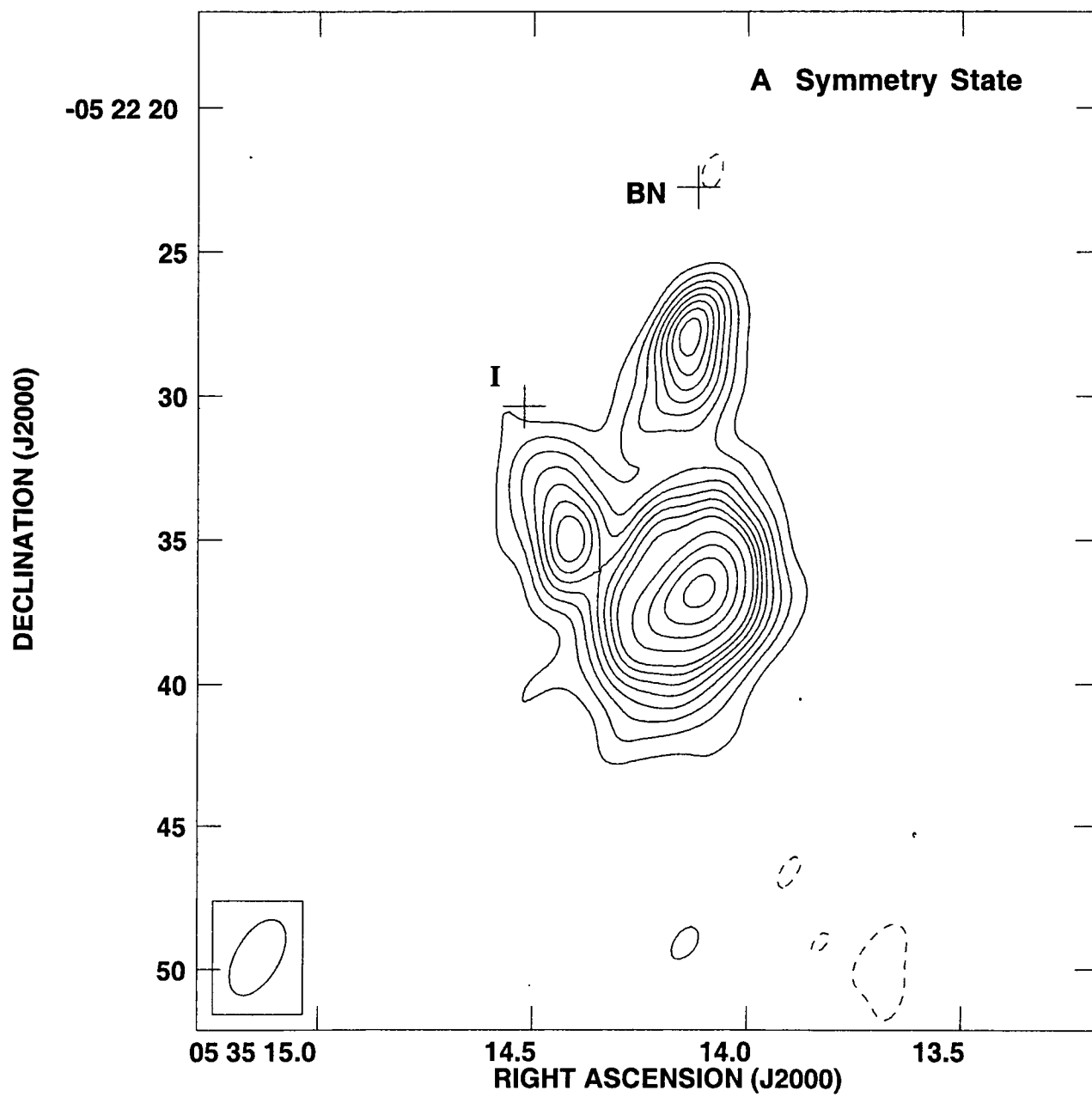


Fig. 2

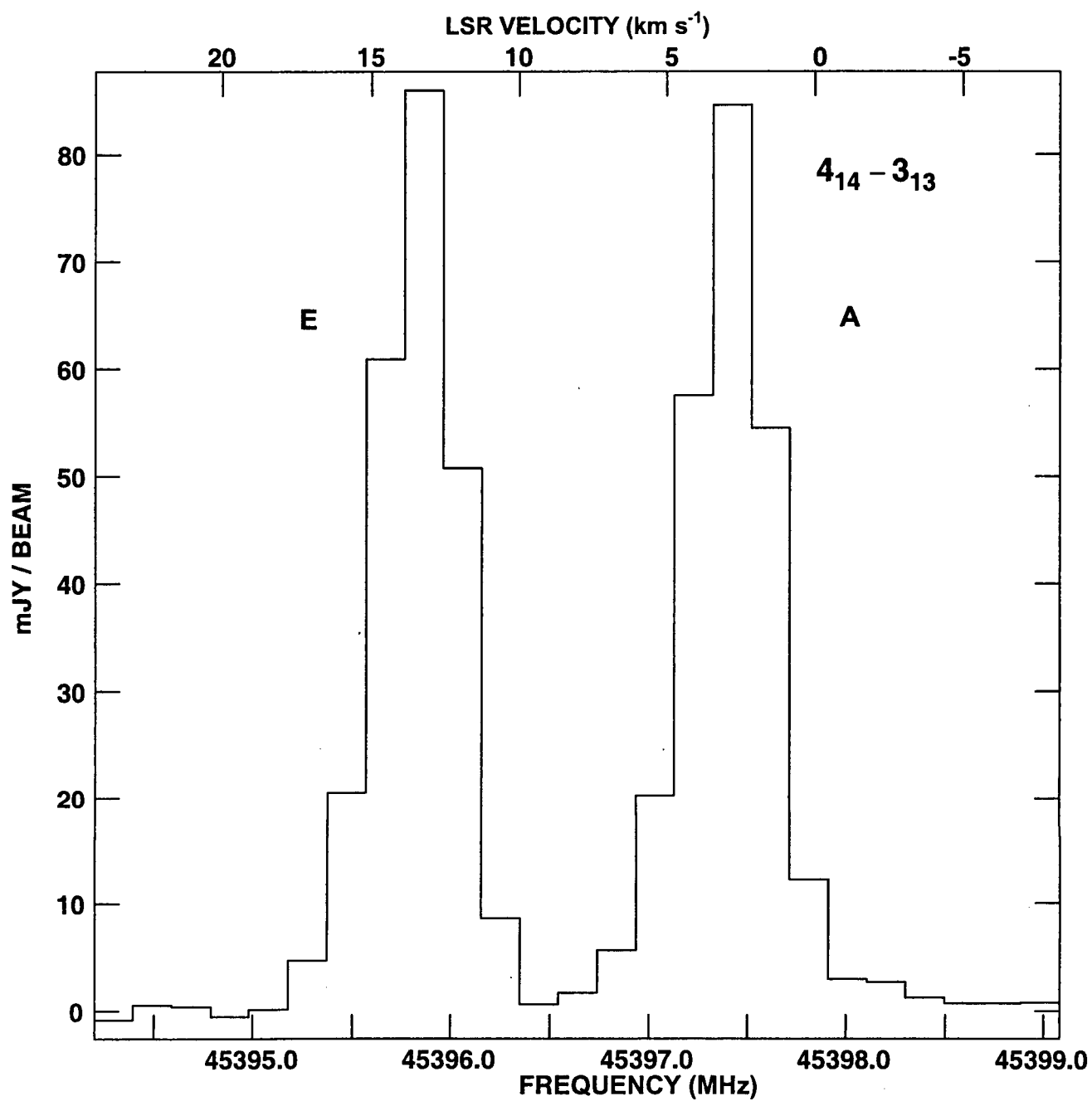


Fig. 3

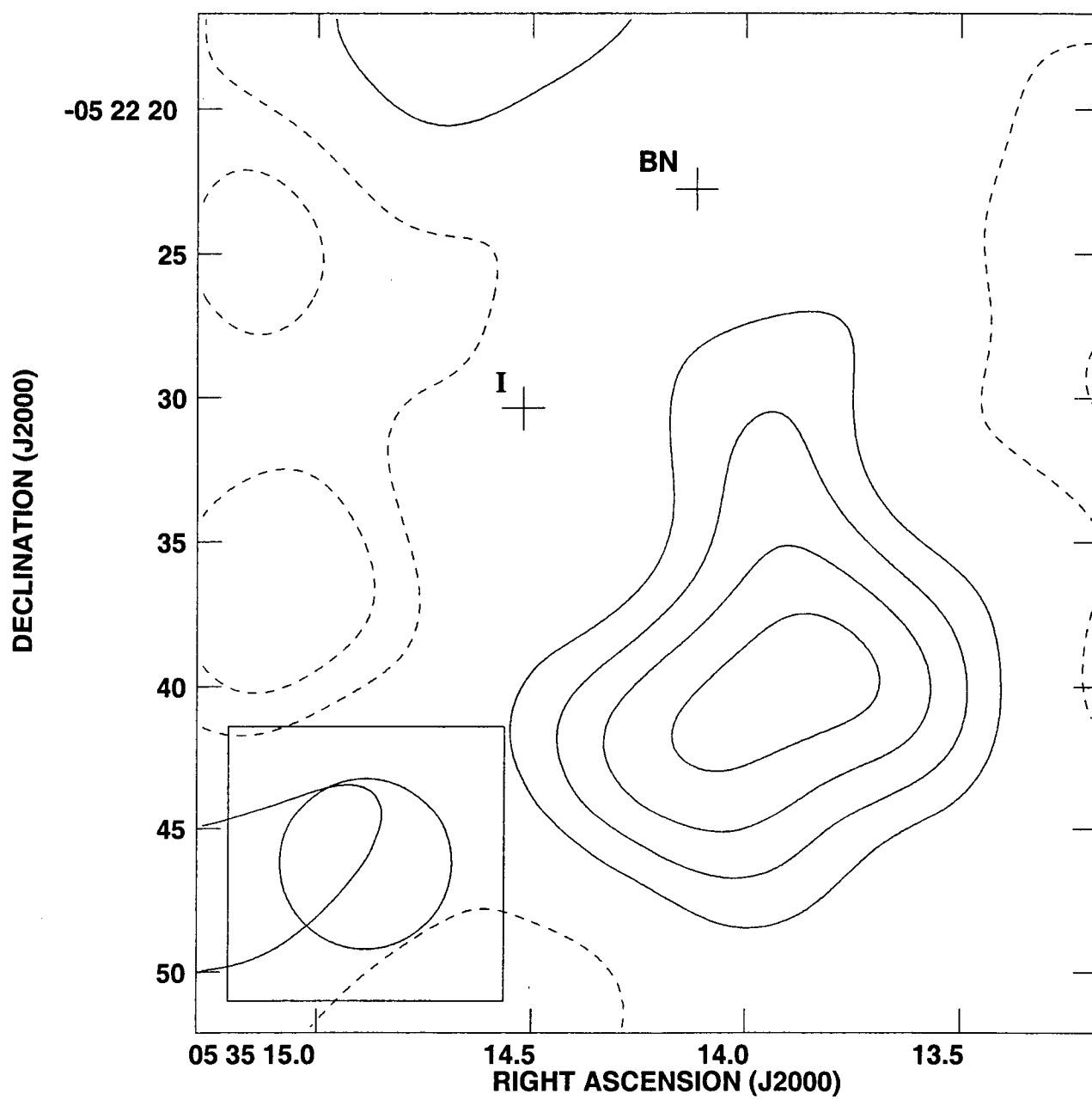




Fig. 4

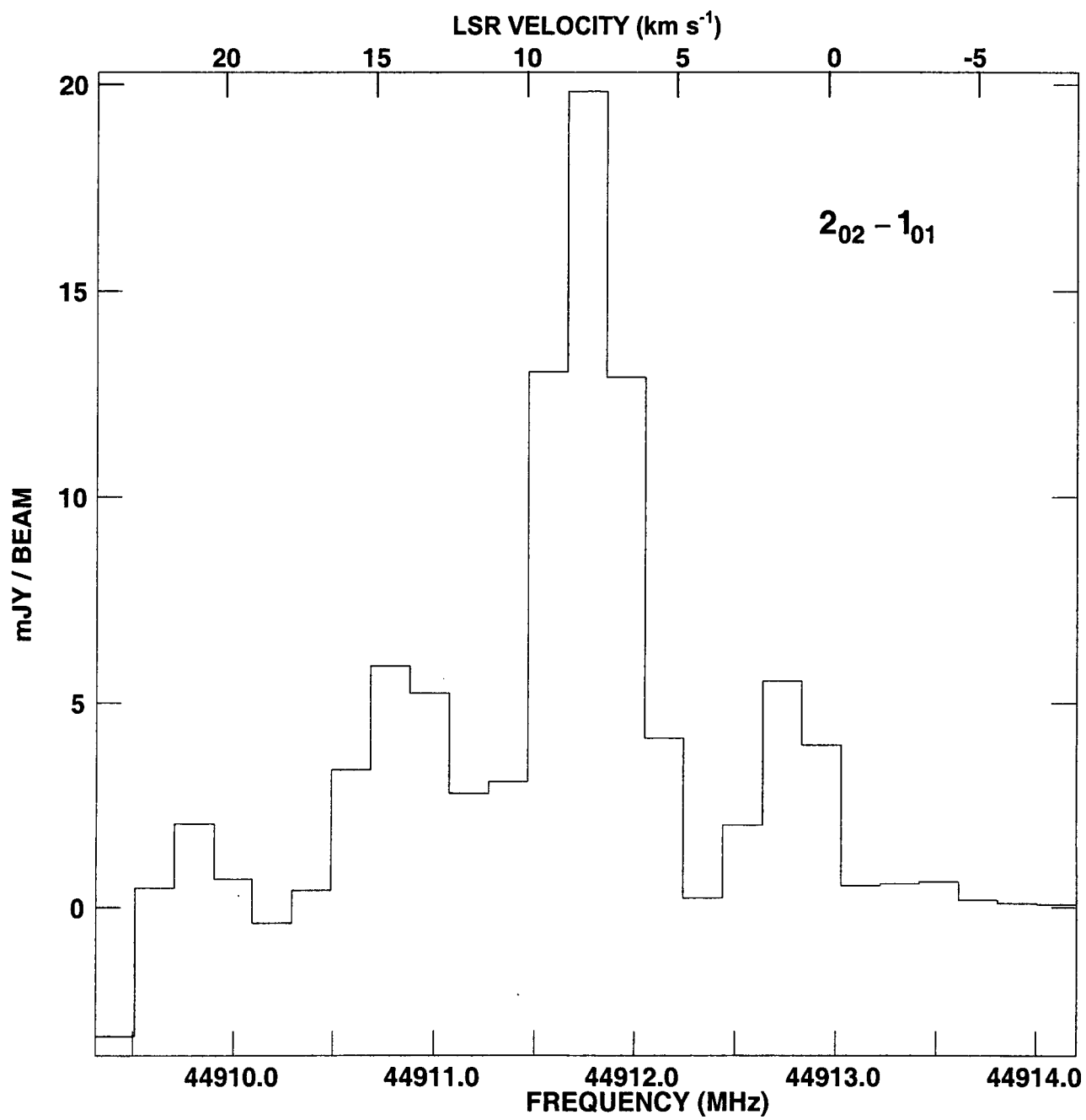


Fig. 5

